A Case Study of Atmospheric Conditions at 4–19 km over Vandenberg Air Force Base during Passage of a Cyclone

G. D. NASTROM

St. Cloud State University, St. Cloud, Minnesota

F. D. EATON

Air Force Research Laboratory, Kirtland Air Force Base, New Mexico

(Manuscript received 8 March 2002, in final form 29 September 2002)

ABSTRACT

Continuous observations from a 50-MHz radar of the vertical profiles of winds, refractivity turbulence structure constant (C_n^2), turbulent kinetic energy density (σ_t^2), and hourly standard deviation of the vertical velocity (σ_w) are combined with routine rawinsonde ascents and weather observations to study changes in turbulence intensity over Vandenberg Air Force Base, California, during 21–27 July 2001. Early and late in this period the flow aloft was relatively steady and turbulence intensities in the upper troposphere were very low. For about 36 h around 25 July, the flow at midlevels (about 600–150 hPa) was disturbed by the passage of a cutoff cyclonic circulation center. During the low's passage, C_n^2 and σ_t^2 intensities were enhanced by up to about 15 dB. The enhancements of C_n^2 and σ_t^2 are highly correlated with each other, as well as with the vertical shear of the horizontal wind and synoptic-scale relative vorticity. The increased turbulence intensities apparently are due to in situ processes, such as shear instabilities associated with the low. Brief episodes of enhanced σ_w, taken as an indicator of enhanced gravity wave activity, are also associated with the low's passage, and they are also apparently due to an in situ process, such as shear instability or geostrophic adjustment. In the lower stratosphere, above 16 km, winds show a periodic oscillation, with a period near the local inertial period and with downward phase progression. There are bursts of enhanced C_n^2 near the lower edge of this oscillation. The oscillation does not appear to be affected by the low's passage.

1. Introduction

The 50-MHz radar wind profiler recently installed at Vandenberg Air Force Base (AFB) (VBG), California, was operated continuously for a brief campaign from 2000 UTC 20 July to 0000 UTC 28 July 2001. During this period a closed, cold-core, cyclonic circulation system in the upper troposphere passed directly over VBG. Although closed lows represent a major class of circulation features at midlatitudes, there have been relatively few studies of their detailed structure using mesosphere–stratosphere–troposphere (MST) radars. MST radar observations can provide high temporal and vertical resolution sampling of both horizontal and vertical winds, as well as measurements of turbulence intensity. Past studies of cutoff lows using MST radar data have considered the changes to the mean horizontal and vertical wind fields (Fukao et al. 1989), and to the tropopause as seen by the aspect ratio of the vertical to oblique returned power (e.g., Caccia et al. 2000, and references therein). The present study will focus on the changes to the turbulence intensities and their relationships to the large-scale flow features associated with the low.

The results from VBG are of special interest for several reasons. Closed lows are often associated with convection and it is thus difficult to distinguish enhancements of turbulence or wave activity due to circulation features within the low, such as wind shears, from those due to convection. Throughout the period studied here the air was very dry over southern California with clear skies, except under the marine inversion along the coast. There were no convective clouds within several hundred kilometers of VBG. Further, the radar at VBG is located only 3 km east of the seashore and locally the boundary layer throughout this period was stable because of the intense marine inversion. Although closed lows are also often associated with strong winds in the lower troposphere, which could launch intense upward-propagating gravity waves if flowing over rough terrain, throughout this period the winds below about 3 km were very light, usually less than 5 m s^{-1}. Thus, the region sampled by the VBG radar (from about 2 to nearly 20 km) was not

Corresponding author address: Dr. G. D. Nastrom, Department of Earth and Atmospheric Science, St. Cloud State University, St. Cloud, MN 56301.
E-mail: nastrom@stcloudstate.edu

influenced by large variations of the intensity of upwelling gravity waves launched in the boundary layer by low-level convection or by variations in the flow over rough terrain. The large changes in turbulence intensities seen during the passage of the cutoff low can be related to changes in features of the flow aloft, such as vertical wind shear, free of the confounding influence of surface-based effects.

The paper is organized as follows: section 2 describes the radar system and data used, section 3 presents the synoptic weather conditions, and section 4 gives the observations and case study results. Section 5 contains a discussion of the results, and a summary and conclusions are given in section 6.

2. Radar system and data used

The radar used in this study is located at 34°46′48″N, 120°33′36″W, at 74 m MSL, about 6 km northwest from the main administrative area of VBG. The radar is about 3 km east of the Pacific Ocean on the northern side of the Point Arguello/Point Conception landform. Although the radar is located in a cleared area of the Lompoc basin, the natural vegetation found on the surrounding terrain is the chaparral forest type typically found in southern California. The terrain to the west, about 200°–330°, slopes gently to the shore. Terrain elevations within 15 km are below 500 m, while roughly 30 km to the east and northeast of VBG the coastal mountains rise to heights in excess of 1 km.

Salient parameters of the VBG MST radar are shown in Table 1. System characteristics are similar to those of the MST radar that was operated at White Sands Missile Range (WSMR), New Mexico, from 1991 to 1997 and described by Nastrom and Eaton (1993). Note that the pointing directions of the two oblique beams are 225° and 315° instead of the conventional cardinal points. This was done to minimize contamination from ocean wave effects.

Doppler spectra were obtained at 3-min intervals on each of the three beams. Vertical profiles of the wind speed, backscattered power [reported as signal-to-noise ratio (SNR) and calibrated as the refractivity turbulence structure constant (C_n^2)], and the Doppler spectral width obtained from the Doppler spectra are used in this study.

The radar data are augmented by rawinsonde ascents and surface weather observations made at VBG within a few kilometers of the radar site. Surface observations from other nearby locations, routine weather map analyses, images from both geostationary and polar orbiting satellites, and weather radar summaries are also used. To further help to characterize atmospheric conditions, output from the mesoscale models available through the Real-time Environmental Applications Display System of the Air Resources Laboratory of the National Oceanic and Atmospheric Administration (NOAA) was used.

TABLE 1. Radar parameters at Vandenberg AFB used in this study.

Component/Parameter	Value
Transmitter	
Nominal frequency	49.25 MHz
Output power	250-kW peak
Duty cycle	5%
Pulse width (compressed)	8 μs (8:1) 1 μs nominal
Type	Combination solid-state preamplifier and tube-cavity amplifier, three stage
Antenna	
Physical aperture	15 600 m^2
Effective aperture	13 500 m^2
Pointing (three beams)	Zenith and 15° at 225° and 315° azimuth
Type	Phased array of coaxial colinear elements
One-way beamwidth	2.9°
Receiver	
Type	Single conversion
Bandwidth	Matched to transmitted pulse
Receiver noise figure	Less than 1 dB
Performance	
Nominal lowest range gate	2 km above ground level
Range-gate spacing	150 m
Time resolution	1 min per beam
No. of range gates	126
Horizontal wind range	$\pm$116 m s^{-1}
Calibrated C_n^2 range	10^{-20}–10^{-13} m$^{-2/3}$
Bandwidth	1 MHz
Power aperture product	1×10^8 W m^2

3. Synoptic weather situation

Because of the quasi-stationary Pacific high, the flow aloft over VBG during July is generally southwesterly (off of the ocean) and a strong low-level inversion persists above the marine boundary layer. Indeed, the presence of a strong low-level inversion throughout the period 21–27 July 2001 is verified by the routine 12-hourly rawinsonde ascents from VBG. Figure 1 gives profiles of potential temperature and relative humidity for each 12-hourly sounding at VBG from 1200 UTC 21 July to 0000 UTC 27 July. All soundings show a very stable layer (a strong inversion) below about 900-m altitude. The potential temperatures at higher altitudes show small variability among the soundings except those from 1200 UTC 24 July to 1200 UTC 25 July when the levels near 6 km are colder than usual. The soundings are highly statically stable, except at 1200 UTC 24 July when there is a layer of reduced stability from about 7 to 9 km, just below the tropopause, which is at 9.3 km. On the other soundings, the tropopause height determined from the World Meteorological Organization (WMO) definition ranges from 13.9 to 15.8 km. There is high relative humidity within the marine boundary layer and much lower values, generally below 30% at higher altitudes throughout this period, except for a layer near 4 km at 1200 UTC 25 July.

Surface hourly weather observations from VBG (not

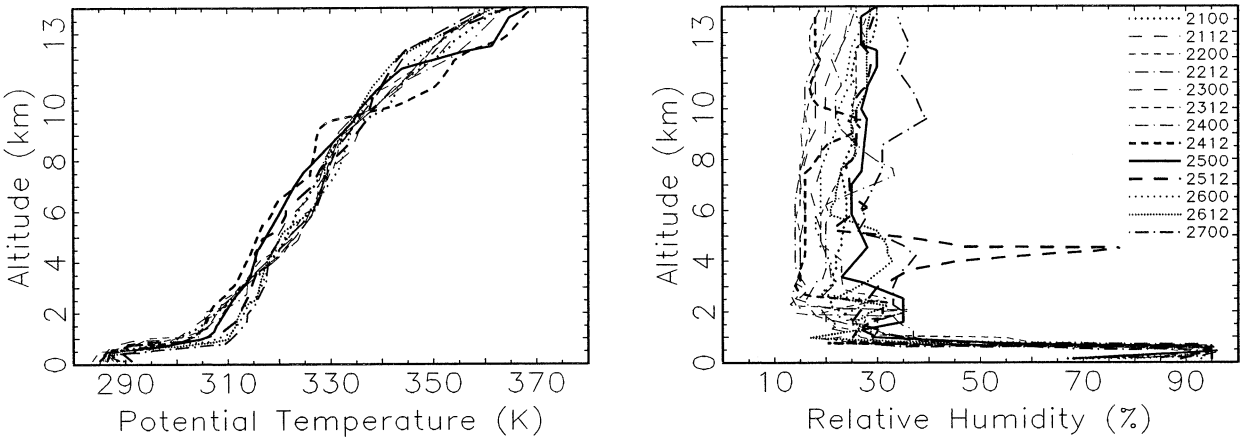

FIG. 1. Vertical profiles of (left) potential temperature and (right) relative humidity from rawinsondes launched at VBG during the period 0000 UTC 21 Jul–0000 UTC 27 Jul 2001.

shown) indicate continuous low cloud ceilings with occasional fog and drizzle throughout this period. The inland extent of the cloud deck in the marine boundary layer oscillated from a few kilometers to a few tens of kilometers from day to night. Surface observations from Santa Maria and San Luis Obispo (both slightly farther inland than VBG) showed overcast conditions during the night and morning and clear conditions in the late afternoon each day. Satellite imagery (e.g., Fig. 2a) shows that the overcast was confined to the coastal regions. Infrared imagery (not shown) indicates that the tops of these clouds were very low. Beneath the overcast, surface winds at VBG were usually 5 m s^{-1} or less, except at 0000 UTC 21 July, when they gusted to 10 m s^{-1} from the northwest.

Farther inland no significant weather was reported during this period. For example, Bakersfield (about 150 km northeast of VBG in the San Joaquin Valley) continuously reported clear skies. Satellite images from the Geostationary Operational Environmental Satellite (GOES) and from *NOAA-12, -14,* and *-16* (about 1400–1700 LST daily) and the hourly weather radar summaries show late afternoon showers (up to about 35 dB*Z*) along the Sierra Nevada, over 250 km east and northeast of VBG, each afternoon from 23 to 26 July.

The satellite water vapor images (e.g., Fig. 2b) show the passage over VBG of a well-formed closed low on 24–25 July. As noted above, there was relatively little moisture aloft, and no mid- or upper-level clouds were associated with this low. The synoptic weather maps confirm the passage of a closed low over VBG during this period. At 400 hPa (about 7.5 km), the maps from NOAA's Air Resources Laboratory Real-time Analysis and Display System show a sharp trough began moving down the coast of Oregon on 23 July as the flow over VBG turned from southwesterly to westerly. The trough deepened and formed into a closed low centered just north of VBG at 1200 UTC 24 July (Fig. 3). On 25 July the low center was found several hundred kilometers east of VBG and the associated winds over VBG had a strong northerly component. By 26 July the remaining weak trough was over Arizona with the flow over VBG being much weaker and from the northwest, consistent with the wind patterns seen in Fig. 4.

Figure 4 gives the vertical profiles of wind speed and direction at VBG corresponding to the soundings in Fig. 1. Below 3 km, wind speeds were usually less than 5 m s^{-1} on all soundings. Above 3 km, winds were persistently from the southwest or west until 0000 UTC 24 July, when they began veering to the northwest as the cutoff low approached. Winds, as the low was passing at 0000 UTC 25 July, were from the north to northeast from about 3 to 6 km and then backed with height to become westerly at 14 km. After the passage of the low the winds above 6 km returned to westerly.

4. Radar observations

Average turbulence intensities were very light during this observing period. Figure 5 shows the oblique-beam hourly median profiles of C_n^2 for all 172 h and the maximum and minimum hourly values found at each altitude. Also plotted in Fig. 5 are the sensitivity limits [called the ''minimum detectable'' limit by Green et al. (1979)] based upon a minimum detectable signal-to-noise ratio of -12 dB. The vertical profile of the minimum C_n^2 values obviously arises from the effects of the sensitivity limits. The apparent discontinuity near 4 km may be due to radar system problems (near-field/far-field transition effects, receiver gain delay, etc.), and we will thus limit discussion of turbulence quantities to above 4 km (however, note that the wind speed measurements should be valid at all altitudes).

The low relative humidity values above the boundary layer during this period indicate that a large part of the variability in C_n^2 is due to turbulence changes. In general, local values of C_n^2 depend both on the intensity of tur-

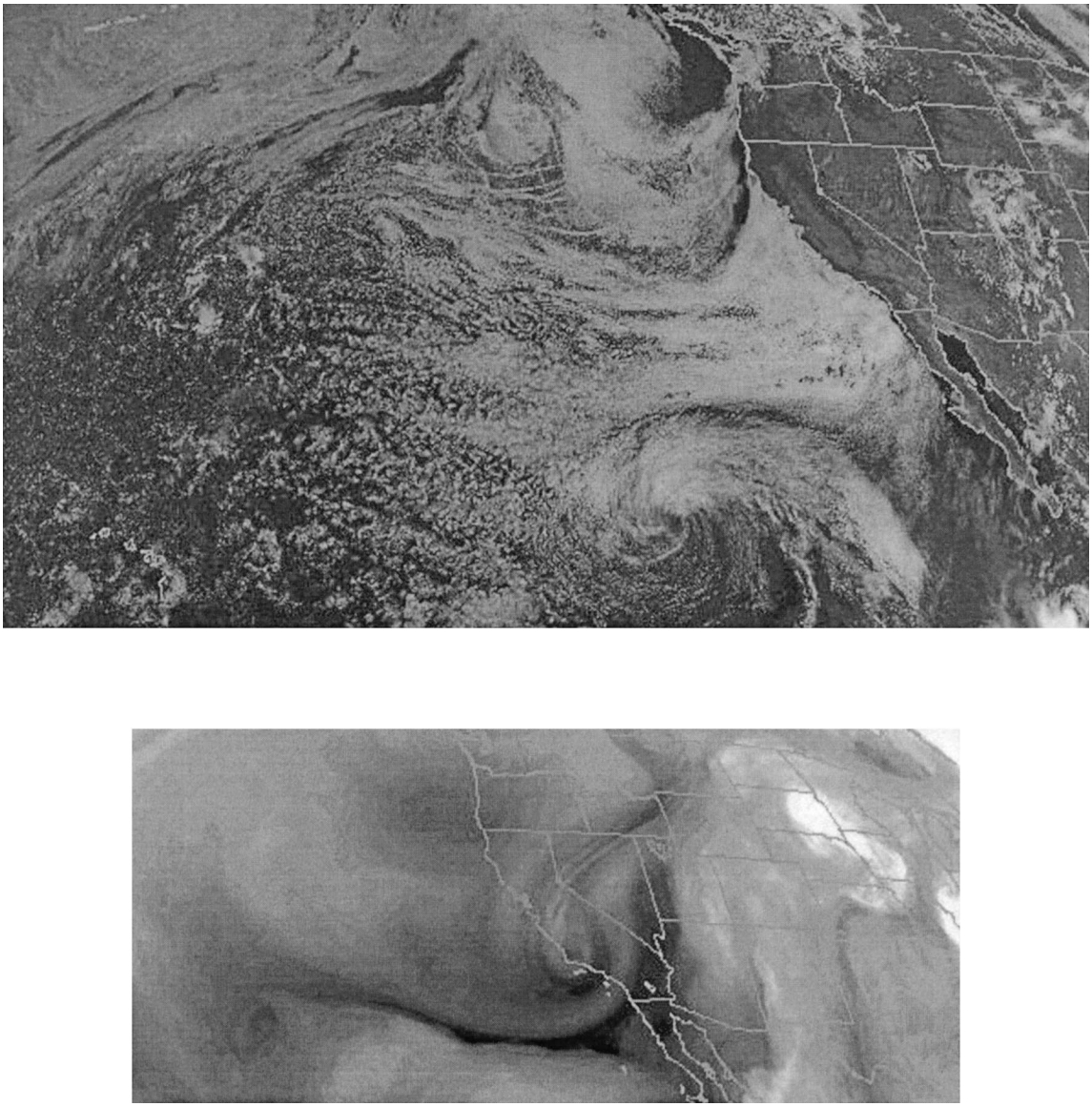

FIG. 2. Satellite images on 24 Jul 2002: (top) visible at 1800 UTC and (bottom) water vapor at 1200 UTC.

bulence through the outer scale of turbulence L_o and on the mean gradient of the refractive index (M),

$$C_n^2 = a^2 \alpha' L_o^{4/3} M^2, \tag{1}$$

where a^2 is a constant and α' is the ratio of eddy diffusivities, usually taken as constant [see Gage (1990) for a review]. In addition, L_o is related to the eddy dissipation rate ε and the wind shear du/dz by $L_o = (\varepsilon/\gamma)^{1/2} |du/dz|^{-3/2}$, where γ is usually taken as constant; M is related to the stability ($d \ln\theta/dz$) and specific humidity (q) as

$$M = -77 \times 10^{-6} \frac{p}{T}\left(\frac{d\ln\theta}{dz} + \frac{15\,500q}{T}\frac{d\ln\theta}{dz} - \frac{7800}{T}\frac{dq}{dz}\right). \tag{2}$$

In the presence of high humidity and humidity gradients, M and hence C_n^2 depend strongly upon humidity (Tsuda et al. 1988). However, the rawinsonde soundings during this period (Fig. 1) indicate that humidity levels were low and uniform with time above about 4 km. The rawinsonde soundings further show that the stability above the boundary layer was fairly uniform with time, except from 7 to 9 km on 1200 UTC 24 July. Nastrom and Eaton (2001) show that in the absence of humidity the volume-averaged C_n^2 is proportional only to turbulence intensity and stability, and because the stability changes here were small, the changes in C_n^2 with time were due to changes in turbulence intensity. The high correlations of C_n^2 with wind shear and σ_t^2, to be shown later, support this conclusion.

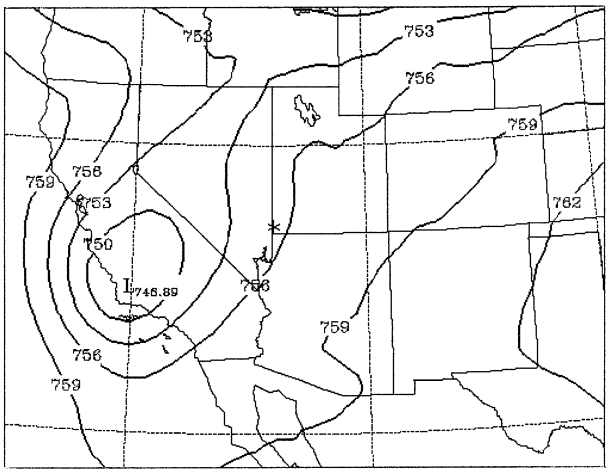

FIG. 3. Geopotential height analysis at 400 hPa at 1200 UTC 24 Jul 2001.

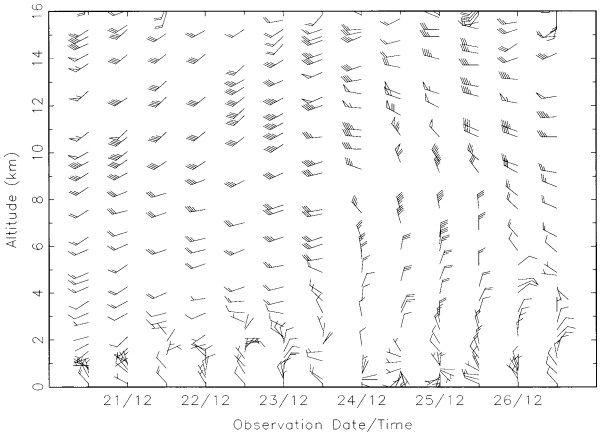

FIG. 4. As in Fig. 1, but for horizontal winds. Scale: no barbs, <1 m s^{-1}; half barb, 2.5 m s^{-1}; full barb, 5 m s^{-1}; flag, 25 m s^{-1}.

The wind patterns seen by the radar are consistent with those from the rawinsonde soundings and weather maps discussed above. The upper panels of Fig. 6 show the hourly medians of horizontal wind speed and direction. For reference, hour 100 corresponds to 0000 UTC 25 July. A wind speed maximum is seen near 12 km at all hours during this period. There are two strong pulses of wind speed, one is over 30 m s^{-1} around 12.5 km at hour 88 (1200 UTC 24 July) and the other is over 35 m s^{-1} from about 9 to 12 km near hour 100. Wind speeds below about 5 km and above 17 km are less than 10 m s^{-1}. In the midtroposphere, the wind direction is from the southwest before about hour 90 and then rapidly swings around to the northwest after hour 95 and then returns to southwesterly after about hour 150. Below about 6 km the winds are from the north-northeast from about hour 90 to 150.

The heights of the tropopause estimated using the rawinsondes launched at 12-h intervals at VBG are shown by circled crosses in all panels of Fig. 6. In the lower panels the points are connected by straight lines to show time progression of the tropopause. The dip near hour 88 coincides with the passage of the upper-tropospheric closed low.

The flow in the stratosphere above 16 km is dominated by a quasi-periodic oscillation that shows downward phase progression with time. The amplitude of this oscillation is about 5 m s^{-1}. The oscillation goes through about eight cycles in 140 h, indicating that its period is near the inertial period for the latitude of VBG (21.1 h). The vertical wavelength is typically slightly less than 2 km, although there is significant variation of vertical wavelengths among cycles. Inertial oscillations have been seen at other MST sites (e.g., Cornish and Larsen 1989; Thomas et al. 1992; Sato et al. 1997). A more detailed investigation of this stratospheric oscillation is beyond the scope of the present study. However, the main point noted here is that this oscillation does not seem to be affected by the strong wind changes in the troposphere during the passage of the upper-tropospheric low.

Turbulence and waves in the troposphere are strongly affected by the passage of the upper-tropospheric low. The lower-right-hand panel of Fig. 6 shows the standard deviation of vertical velocity relative to the hourly mean (σ_w), which is often used as an indicator of the intensity of gravity wave activity. Values typically range from 0.10 to 0.15 m s^{-1}, except for two periods at about 12 km near hour 90 and 100 when they exceed 0.25 m s^{-1}. Even the largest of these values at VBG is relatively small when compared with those typically seen at other sites. For example, Nastrom and Eaton (1995) found the seasonal median hourly values of σ_w at WSMR are about 0.2–0.3 m s^{-1} and Sato (1990) indicates σ_w ranges from 0.2–0.6 m s^{-1} over the middle and upper atmosphere (MU) radar site in Japan. Nastrom et al. (1996) found that seasonal mean values of σ_w range from about 0.15

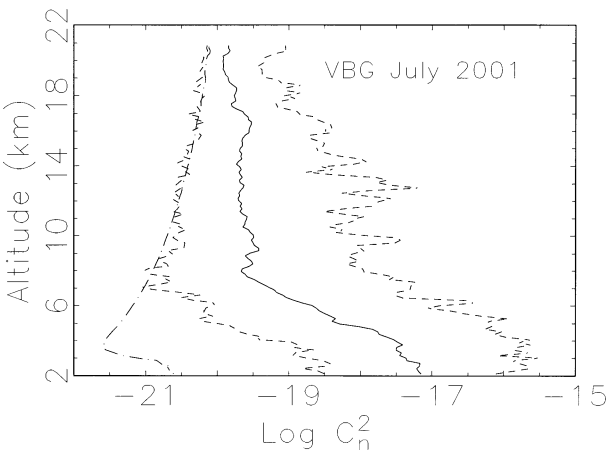

FIG. 5. Vertical profile of the median log C_n^2 at VBG for the 172-h period of this study. The max and min hourly values at each level are given by dashed lines, and the minimum detectable signal (see text) is a chain line.

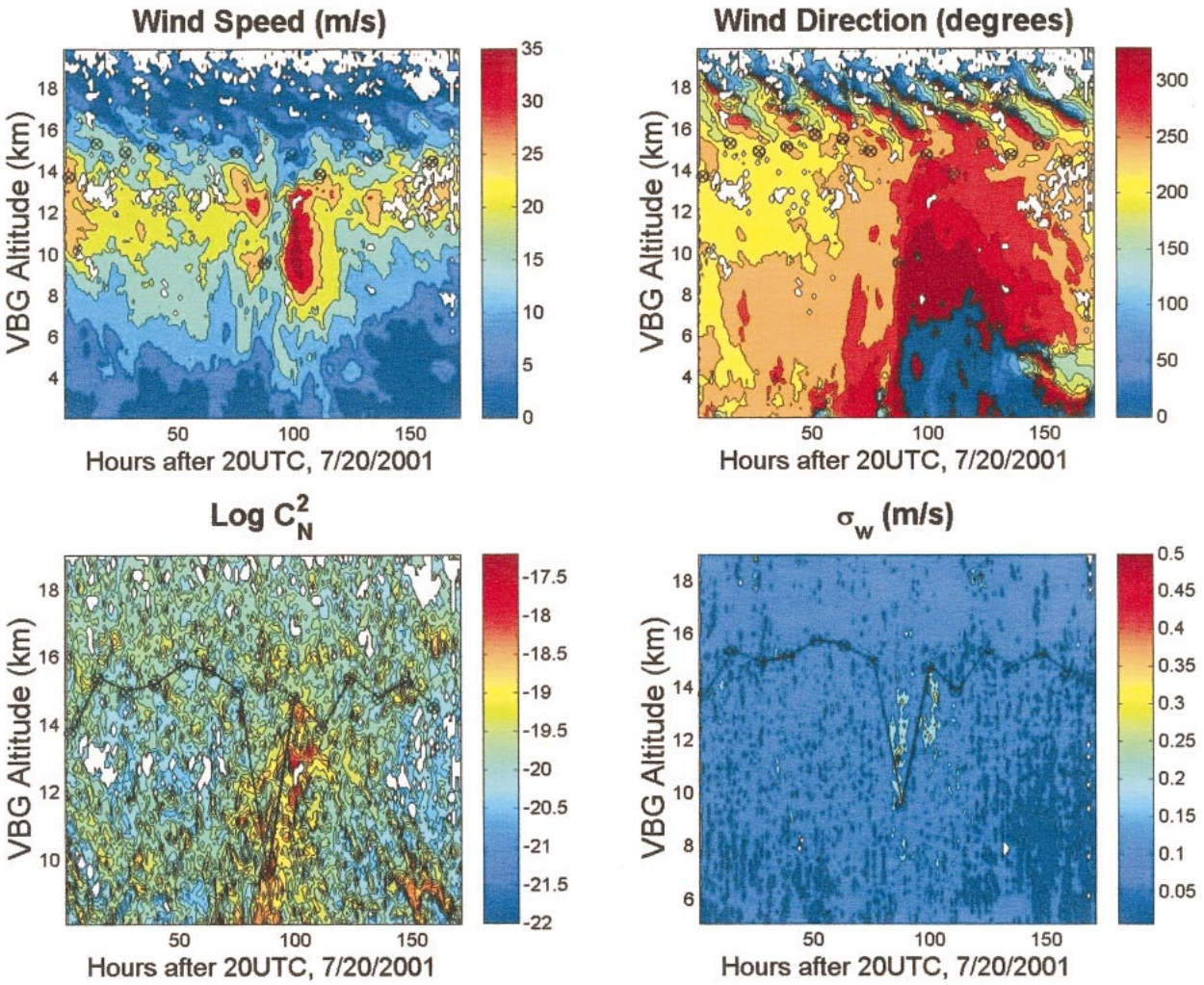

FIG. 6. Height–time plots of (top) the hourly median wind speed and direction, (lower left) log C_n^2, and (lower right) hourly std dev of the vertical velocity at VBG. The tropopause height is indicated at 12-hourly intervals by large dots; for evaluation convenience, the dots are connected in the lower panels.

to 0.2 m s^{-1} over the Flatland radar in the very flat terrain of central Illinois, although the typical values were about 0.10 m s^{-1} when low-level temperature inversions were present. The bursts of enhanced σ_w seen in Fig. 6 coincide with the passage of the closed low as discussed further below.

The lower-left-hand panel of Fig. 6 shows hourly medians of logC_n^2 above 8 km. The main feature is the enhancement of C_n^2 up to about 15 km during approximately hours 75–115, that is, near the time of the passage of the closed low. The magnitudes of the enhancements are 10–15 dB, with occasional values over 20 dB above the background. The enhanced values appear progressively later with increasing altitude, approximately parallel to the times of trough axis passage at VBG. At 300 hPa (about 9.5 km), the trough axis passed at about 1200 UTC 24 July, and at 150 hPa (about 14 km) it passed at about 0300 UTC 25 July. Because the atmosphere above about 6 km was very dry during this period (Fig. 1), the enhanced C_n^2 values indicate enhanced turbulence on the scale of one-half of the radar wavelength (3 m).

Another interesting feature in Fig. 6 is the frequent enhancement of C_n^2 between about 16 and 17 km. Although individual episodes of enhancement are up to 10 dB over periods of several hours and extend up to 1 km in the vertical, they are not all at the same height (thus, the relative enhancement with the height of the median C_n^2 near 17 km in Fig. 5 is smeared with altitude and has a maximum value only about 3 dB). Figure 6 shows that the enhancements are usually located 1–2 km above the tropopause, near the lower edge of the quasi-periodic stratospheric oscillation. The enhancements of C_n^2 in the stratosphere are not unusual when the closed low passes. At first glance the enhancements of C_n^2 appear to be related to the increased vertical shears of the horizontal wind due to the quasi-periodic stratospheric oscillation. However, the episodes of maximum C_n^2 are not always

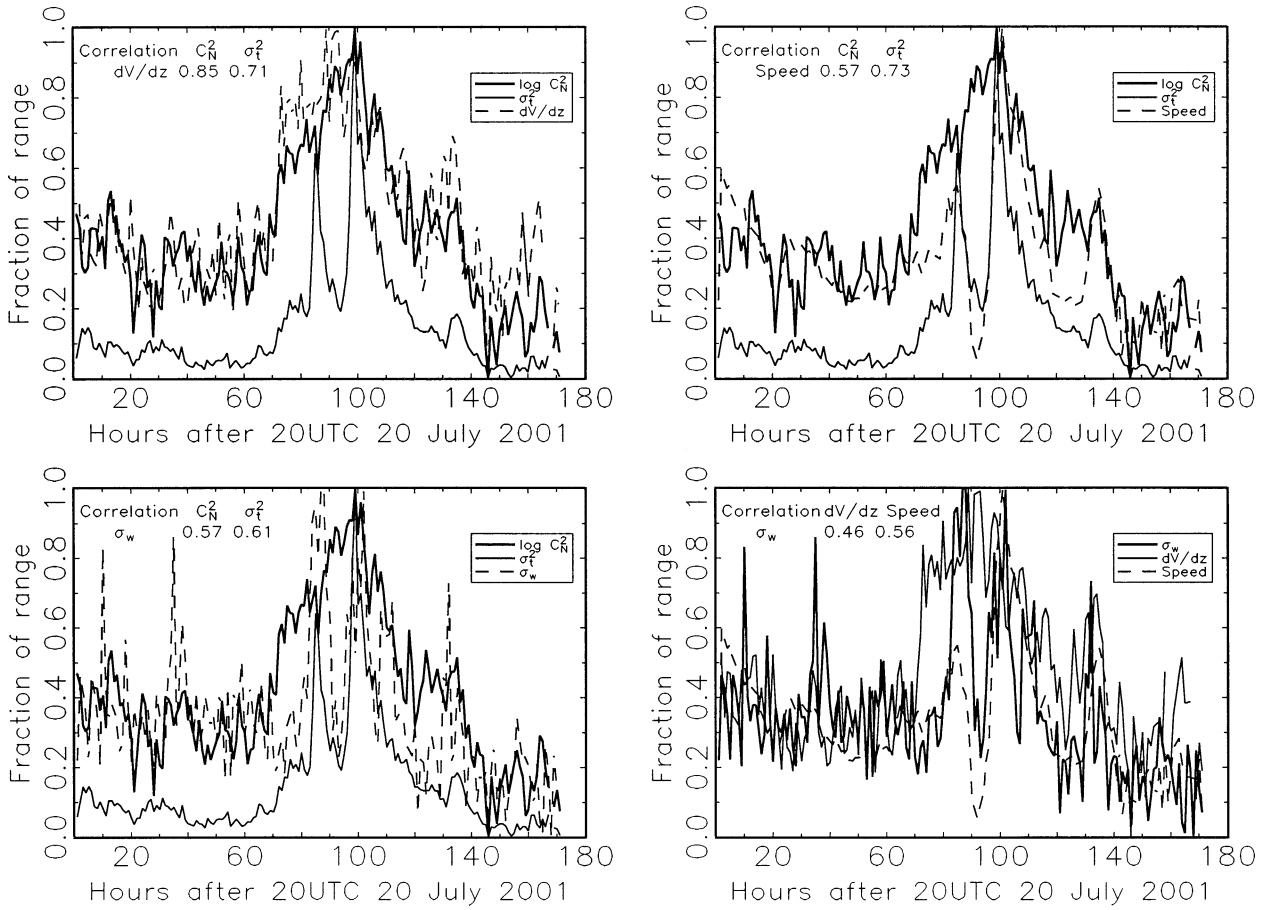

FIG. 7. Comparisons of the time series of hourly averages over the 10–13 km interval of $\log C_n^2$ and σ_t^2 with (top left) vertical shear of the horizontal wind, (top right) wind speed, and (lower left) σ_w; (lower right) comparison of σ_w with mean dV/dz and wind speed.

coincident with those of maximum shear, suggesting another process is also important. One suggestion is that upward-propagating gravity waves experiencing changes in vertical wavelength as a result of crossing the tropopause (VanZandt and Fritts 1989) interact with the shear of the background flow and induce local instabilities.

5. Discussion

Direct measurements of turbulence and wave intensities by MST radars are limited to only a few locations globally. Turbulence intensities are of interest for a variety of applications, such as aircraft safety concerns and effects on electromagnetic propagation in the atmosphere, and are directly related to the turbulence eddy dissipation rate ε, which is a key variable of the general circulation and may play an increasingly important role in future mesoscale models, as discussed by Businger and Businger (2001). Because direct measurements of turbulence intensities are relatively rare, they are often parameterized in terms of other more readily available variables. For example, the pioneering model by Hufnagel (1974) used wind speed over a broad layer as a predictor for C_n^2.

TABLE 2. Max and min values of variables shown in Fig. 7.

Variable	Max	Min	Range
$\text{Log}C_n^2$	−18.66	−20.42	1.76
σ_t^2 (m^2 s^{-2})	1.18	0.12	1.06
Wind speed (m s^{-1})	36.5	15.0	21.5
dV/dz [m s^{-1} (300 m)$^{-1}$]	4.09	0.290	3.80
σ_w (m s^{-1})	0.217	0.085	0.132
ζ_{300} (10^{-5} s^{-1})	14.0	−1.75	15.75
ζ_{200} (10^{-5} s^{-1})	10.5	−2.50	13.0

Figure 7 compares the time series of the hourly median values at 10–13 km of $\log C_n^2$ and σ_w with the wind speed and the vertical shear of the horizontal wind $\{dV/dz = [(du/dz)^2 + (dv/dz)^2]^{1/2}$, where $dz = 300$ m$\}$. The turbulent kinetic energy, σ_t^2, estimated from the spectral width after correction for beam-, shear-, and wave-broadening effects as described by Nastrom and Eaton (1997), is also included in Fig. 7. The curves in Fig. 7 are all normalized to have unity range; the maximum and minimum values of each variable are given in Table 2. The correlation coefficients of the 172 hourly pairs,

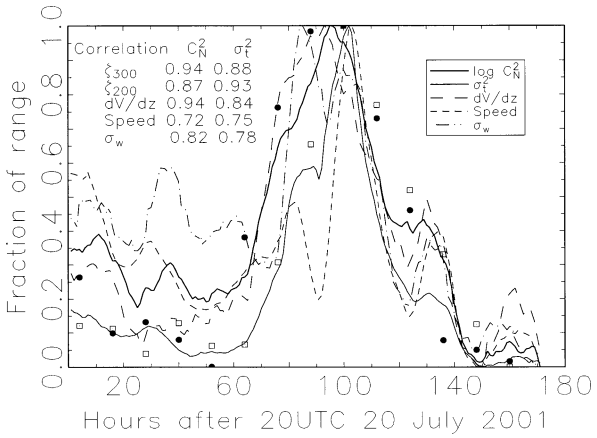

FIG. 8. As in Fig. 7, except curves are smoothed by 12-h running means and correlation coefficients are computed using only points at 0000 and 1200 UTC daily. Relative vorticity at 300 hPa (200 hPa) is shown by dots (boxes), respectively.

given in Fig. 7, range between 0.85 (C_n^2 vs dV/dz) and 0.46 (σ_w vs dV/dz). The correlation coefficient between C_n^2 and σ_t^2 is 0.81. There is smaller correlation between turbulence (C_n^2 and σ_t^2) and wave intensity (σ_w).

For the hourly values during this period, dV/dz is the best predictor for C_n^2 and is nearly the best predictor for σ_t^2. Because direct measurements of the horizontal wind and its small-scale vertical shear are available only at a relatively small number of rawinsonde sites globally, and usually only at 12-hourly intervals, it is interesting to search also for a predictor based on the large-scale flow. Figure 8 compares the time series smoothed with a 12-hourly running mean. Also included in Fig. 8 are the values of the vertical component of the relative vorticity ($\zeta = \partial v/\partial x - \partial u/\partial y$) at 300 and 200 hPa. The correlation coefficients with C_n^2 and σ_t^2, computed using only values at 0000 and 1200 UTC daily, are included in Fig. 8. The relative vorticity is an excellent predictor of both C_n^2 and σ_t^2 in this case study. Because relative vorticity is easily obtained from weather maps or numerical model output, this result suggests that future studies should explore the relationship between turbulence intensity and vorticity more thoroughly than is possible in this case study.

The relative vorticity is determined from horizontal wind shears. The present correlation results thus support the suggestion that the changes in turbulence (both refractivity turbulence and mechanical turbulence) are due to in situ dynamic instabilities related to horizontal and vertical wind shears associated with the cyclone. It seems unlikely that they are related to increased gravity wave activity upwelling from the boundary layer because there is no evidence of increased low-level convection or of strong changes in the wind flow across the terrain with the passage of the low.

6. Summary

The 50-MHz radar at Vandenberg AFB, California, was operated continuously for about 172 h during July 2001. During this period a cold-core closed low in the mid- and upper troposphere passed over the radar site, causing significant changes to the winds aloft. The atmosphere above the marine boundary layer remained dry, free of clouds and significant convection, as the low passed. Wind speeds at and below the heights of the surrounding terrain were light throughout the period. The following points were noted:

1) Indicators of the small-scale turbulence intensity (C_n^2 and σ_t^2) were enhanced by up to about 15 dB in the mid- and upper troposphere around the time of passage of the low, relative to earlier and later periods. The enhanced C_n^2 values appeared successively later with increased altitude, corresponding to the later times of trough passage with altitude.
2) Changes in the hourly values of C_n^2 and σ_t^2 during this period are closely correlated with the vertical shear of the horizontal wind. They are also closely correlated with the vertical component of the relative vorticity. Because vorticity is readily available from large-scale weather analyses, this result suggests that vorticity should be explored more thoroughly as a predictor for small-scale turbulence intensities.
3) The hourly standard deviation of vertical velocity, taken as an indicator of gravity wave intensity, was very small (similar to that seen over the Flatland site in Illinois) except during the passage of the closed low. The brief enhancements of σ_w at these times are apparently associated with gravity waves generated by in situ processes, such as geostrophic adjustment and/or shear instability, rather than surface-based processes.

Acknowledgments. GDN was partially supported by NSF Grant ATM-0129464 and the Air Force Office of Scientific Research.

REFERENCES

Businger, S., and J. A. Businger, 2001: Viscous dissipation of turbulence kinetic energy in storms. *J. Atmos. Sci.,* **58,** 3793–3796.

Caccia, J.-L., F. Bertin, B. Campistron, V. Klaus, Y. Pointin, J. van Baelen, and R. Wilson, 2000: Cut-off low monitoring by the French VHF-ST-radar network during the ESTIME campaign. *J. Atmos. Solar-Terr. Phys.,* **62,** 639–651.

Cornish, C. R., and M. F. Larsen, 1989: Observations of low-frequency gravity waves in the lower stratosphere over Arecibo. *J. Atmos. Sci.,* **46,** 2428–2439.

Fukao, S., M. D. Yamanaka, H. Matsumoto, T. Sato, T. Tsuda, and S. Kato, 1989: Wind fluctuations near a cold vortex-tropopause funnel system observed by the MU radar. *Pure Appl. Geophys.,* **130,** 463–479.

Gage, K. S., 1990: Radar observations of the free atmosphere: Structure and dynamics. *Radar in Meteorology,* D. Atlas, Ed., Amer. Meteor. Soc., 534–565.

Green, J. L., K. S. Gage, and T. E. VanZandt, 1979: Atmospheric measurements by VHF pulsed Doppler radar. *IEEE Trans. Geosci. Electron.,* **GE-17,** 262–280.

Hufnagel, R. E., 1974: Variations of atmospheric turbulence. *Digest of Technical Papers, Topical Meeting on Optical Propagation through Turbulence,* Optical Society of America, Wal-1–Wal-4.

Nastrom, G. D., and F. D. Eaton, 1993: The coupling of gravity waves and turbulence at White Sands, New Mexico, from VHF radar observations. *J. Appl. Meteor.,* **32,** 81–87.

——, and ——, 1995: Variations of winds and turbulence seen by the 50-MHz radar at White Sands Missile Range, New Mexico. *J. Appl. Meteor.,* **34,** 2135–2148.

——, and ——, 1997: Turbulence eddy dissipation rates from radar observations at 5–20 km at White Sands Missile Range, New Mexico. *J. Geophys. Res.,* **102,** 19 495–19 506.

——, and ——, 2001: Persistent layers of enhanced C_n^2 in the lower stratosphere from VHF radar observations. *Radio Sci.,* **36,** 137–149.

——, W. L. Clark, T. E. VanZandt, and J. M. Warnock, 1996: Seasonal and diurnal changes in wind variability from Flatland VHF profiler observations. *Contrib. Atmos. Phys.,* **69,** 5–12.

Sato, K., 1990: Vertical wind disturbances in the troposphere and lower stratosphere observed by the MU radar. *J. Atmos. Sci.,* **47,** 2803–2817.

——, D. J. O'Sullivan, and T. J. Dunkerton, 1997: Low-frequency inertia-gravity waves in the stratosphere revealed by three-week continuous observation with the MU radar. *Geophys. Res. Lett.,* **24,** 1739–1742.

Thomas, L., T. Pritchard, and I. Astin, 1992: Inertia-gravity waves in the troposphere and lower stratosphere. *Ann. Geophys.,* **10,** 690–697.

Tsuda, T., P. T. May, T. Sato, S. Kato, and S. Fukao, 1988: Simultaneous observations of reflection echoes and refractive index gradient in the troposphere and lower stratosphere. *Radio Sci.,* **23,** 655–665.

VanZandt, T. E., and D. C. Fritts, 1989: A theory of enhanced saturation of the gravity wave spectrum due to increases in atmospheric stability. *Pure Appl. Geophys.,* **130,** 399–420.